



Article

Spatiotemporal Evolution Features of the 2022 Compound Hot and Drought Event over the Yangtze River Basin

Lilu Cui ^{1,*},[†] , Linhao Zhong ^{1,†}, Jiacheng Meng ¹, Jiachun An ^{2,3} , Cheng Zhang ⁴ and Yu Li ¹

¹ School of Architecture and Civil Engineering, Chengdu University, Chengdu 610106, China

² Chinese Antarctic Center of Surveying and Mapping, Wuhan University, Wuhan 430079, China

³ Key Laboratory of Polar Environment Monitoring and Public Governance (Wuhan University), Ministry of Education, Wuhan 430079, China

⁴ College of Geomatics, Xi'an University of Science and Technology, Xi'an 710054, China

* Correspondence: cuililu@cdu.edu.cn; Tel.: +86-181-2187-1356

[†] These authors contributed equally to this work.

Abstract: A rare compound hot and drought (CHD) event occurred in the Yangtze River Basin (YRB) in the summer of 2022, which brought serious social crisis and ecological disaster. The analysis of the causes, spatiotemporal characteristics and impacts of this event is of great significance and value for future drought warning and mitigation. We used the Gravity Recovery and Climate Experiment (GRACE)/GRACE Follow-On (GRACE-FO) data, meteorological data, hydrological data and satellite remote sensing data to discuss the spatiotemporal evolution, formation mechanism and the influence of the CHD event. The results show that the drought severity caused by the CHD event was the most severe during 2003 and 2022. The CHD event lasted a total of five months (from July to November), and there were variations in the damage in different sub-basins. The Wu River Basin (WRB) is the region where the CHD event lasted the longest, at six months (from July to December), while it also lasted four or five months in all the other basins. Among them, the WRB, Dongting Lake Rivers Basin (DLRB) and Mainstream of the YRB (MSY) are the three most affected basins, whose hot and drought severity values are 7.750 and -8.520 (WRB), 7.105 and -9.915 (DLRB) and 6.232 and -9.143 (MSY), respectively. High temperature and low precipitation are the direct causes of the CHD event, and the underlying causes behind this event are the triple La Niña and negative Indian Ocean Dipole event. The two extreme climate events made the Western Pacific Subtropical High (WPSH) unusually strong, and then the WPSH covered a more northerly and westerly region than in previous years and remained entrenched for a long period of time over the YRB and its adjacent regions. Moreover, this CHD event had a devastating impact on local agricultural production and seriously disrupted daily life and production. Our results have implications for the study of extreme disaster events.

Keywords: hot; drought; Yangtze River Basin; GRACE/GRACE-FO; extreme climate



Citation: Cui, L.; Zhong, L.; Meng, J.; An, J.; Zhang, C.; Li, Y. Spatiotemporal Evolution Features of the 2022 Compound Hot and Drought Event over the Yangtze River Basin. *Remote Sens.* **2024**, *16*, 1367. <https://doi.org/10.3390/rs16081367>

Academic Editors: John Kalogiros, Jianzhong Lu and Marios Anagnostou

Received: 18 February 2024

Revised: 6 April 2024

Accepted: 11 April 2024

Published: 12 April 2024



Copyright: © 2024 by the authors. Licensee MDPI, Basel, Switzerland. This article is an open access article distributed under the terms and conditions of the Creative Commons Attribution (CC BY) license (<https://creativecommons.org/licenses/by/4.0/>).

1. Introduction

With the rapid development of the social economy and the continuous growth of the population, the global climate and environmental problems are becoming increasingly serious, and the contradiction between supply and demand regarding water resources is becoming more and more prominent. It has led to an increase in global aridity, and the frequency and intensity of droughts are also increasing [1–3]. Frequent droughts have seriously threatened global and regional water security, ecological security and food security [4,5]. The annual global economic damage caused by droughts has soared from USD 17.3 billion in 1980–2009 to USD 23.1 billion in 2010–2017, a rate of increase far greater than for damage caused by other natural disasters [6]. Therefore, it has long been a goal pursued by scientists from all over the world to realize the early warning of drought and monitor the development process of drought.

In the summer of 2022, the Yangtze River Basin (YRB) experienced the most comprehensive high temperature (TEM) process. The abnormal high-TEM event lasted for a long time and was extremely extreme [7]. From July to August, the average precipitation (PPT) in the YRB was 143.2 mm, which is 50.2% less than the same period in previous years [8]. Due to the decreased PPT and high TEM, evapotranspiration (ET) increased greatly, reducing the inflow of rivers by 20%–80%. The compound hot and drought (CHD) event had a serious impact on the local water resources, ecological environment and industrial and agricultural production. In previous studies, the drought index has often been used as a criterion for determining whether a drought has occurred, as well as to quantify the drought severity. Usually, drought is a water shortage for some region due to a lack of PPT. PPT is therefore included in the drought index either alone or together with other meteorological elements, such as the standardized PPT index (SPI), the standardized PPT ET index (SPEI) and the self-calibrating Palmer drought severity index (SCPDSI) [9]. The above meteorological data are investigated mainly through ground-based station and remote sensing techniques. However, the above approaches are not suitable for the fine assessment of the severity and spatiotemporal evolution process of droughts, which is attributed to the sparse distribution of ground stations (ground-based measurement) and the inability to capture complete terrestrial water storage change (TWSC) information (remote sensing) [10–12].

The successful implementation of the Gravity Recovery and Climate Experiment (GRACE) and Follow-On (GRACE-FO) missions has revolutionized the research on drought, allowing scientists to capture drought-induced TWSC with unprecedented precision [13]. Terrestrial water storage is the sum of surface water, soil moisture (SM), snow and ice, vegetation water and groundwater, which is a good quantitative tool for evaluating the spatiotemporal variation characteristics of droughts [14]. Therefore, drought indices based on GRACE/GRACE-FO TWSC were widely used for drought monitoring and quantification [15–18]. Zhang et al. [19] applied GRACE terrestrial water storage change (TWSC) to construct the water storage deficit index (WSDI) in the YRB during 2003 and 2012, and the WSDI was used to detect the drought events in the YRB. The results indicate that low PPT, high TEMs and intense human activity are the main causes of frequent droughts in the YRB. The GRACE-based total storage deficit index was utilized to characterize the spatiotemporal evolution of droughts in Southwest China during 2003 and 2016, and the drought results obtained via the index are more consistent with the drought information reported by the government than the SPEI, SPI and SCPDSI [20]. Sun et al. [21] calculated the WSDI time series of the YRB from 2003 to 2015, and the WSDI found that severe drought events occurred in the YRB in 2004, 2006 and 2011, whose drought severity values reach -2.05 , -2.38 and -1.30 , respectively. The GRACE/GRACE-FO-based drought index can well reflect the occurrence and development of drought in the middle and lower reaches of the YRB in the summer and fall of 2019 [22]. Chao et al. [23] indicated that the WSDI can effectively identify drought events in the YRB and accurately quantify the drought characteristics.

However, this event is not a simple drought but a CHD event, so its formation mechanism and evolution process are more complex and variable. Therefore, it is not comprehensive to study this event only from the perspective of drought. In this study, we innovatively combined geodetic techniques with meteorological and remote sensing approaches to discuss and analyze the formation mechanism and evolutionary characteristics of this CHD event. The primary objectives of this study are the following: (1) to reduce the uncertainty of TWSC from GRACE/GRACE-FO solutions in the YRB; (2) to analyze the spatiotemporal evolution characteristics of the CHD event; (3) to discuss the cause of the CHD event and the drought impacts in the different sub-basins of the YRB; and (4) to analyze the connection between extreme climatic conditions and the CHD event. In our paper, Sections 2 and 3 introduce the study area, data and methods, respectively. Section 4 details the results and their analysis. Sections 5 and 6 are the discussion and conclusion, respectively.

2. Study Area

The YRB (Figure 1) spans 11 provincial administrative regions, with well-developed water systems and abundant water resources (975.5 billion m³). It is the main water source for one-third of China's population and is also an important grain-producing region in China [24,25]. The average annual TEMs in the region range from 16 °C to 18 °C, and the average annual PPT is 1067 mm. The river basin is rich in hydropower resources, and the upstream region is the main power generation region for the West to East Power Transmission [26]. This basin spans the three steps of China's topography, with various types of landforms and complex climate conditions, including the three major climate zones of the Qinghai–Tibet Plateau alpine region, the Southwest tropical monsoon region and the Central China subtropical monsoon region [27]. In our study, we divide the YRB into nine sub-basins, namely the Jingsha River Basin (JSRB), Yalong River Basin (YLRB), Min River Basin (MRB), Jialing River Basin (JRB), Han River Basin (HRB), Wu River Basin (WRB), Dongting Lake Rivers Basin (DLRB), Poyang Lake Rivers Basin (PLRB) and Mainstream of the YRB (MSY).

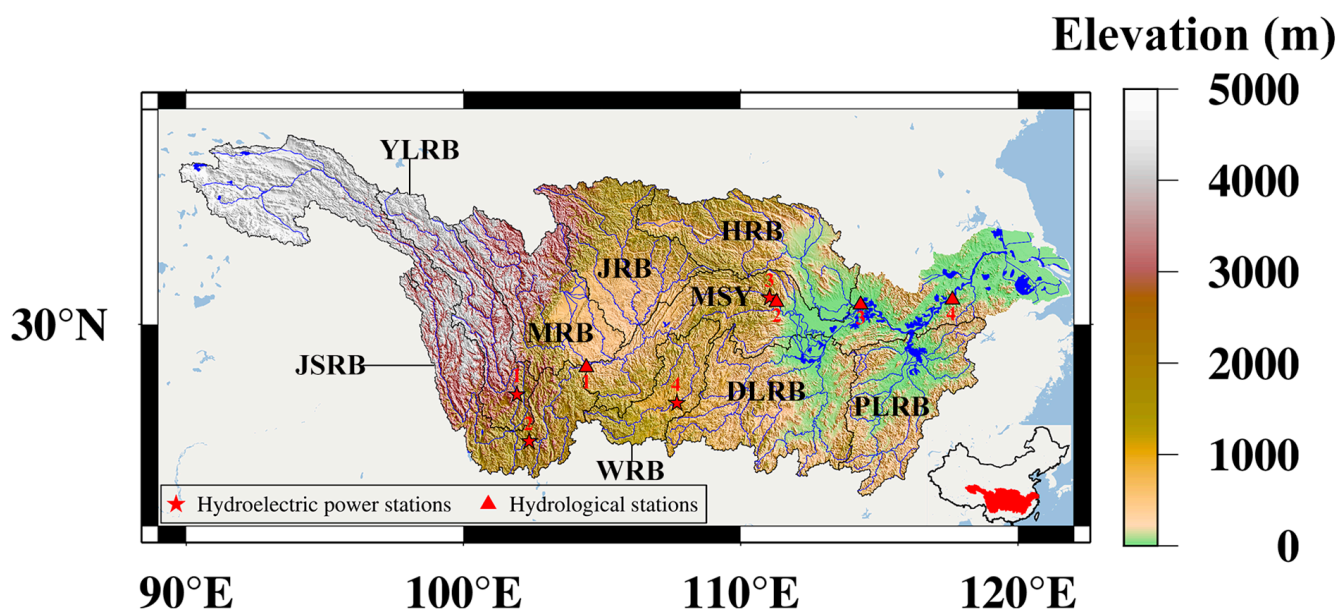


Figure 1. Topographic features and the main sub-basins of the YRB. The name of No. 1-4 hydroelectric power station and hydrological stations are shown in Table 1.

Table 1. List of hydrological and hydroelectric power stations.

Station Number ID	Hydrological Station's Name	Hydroelectric Power Station's Name
1	Xiangjiaba	Jinping
2	Yichang	Xiluodu
3	Hankou	Three Gorges
4	Datong	Goupitan

3. Data and Methods

3.1. Data

3.1.1. GRACE/GRACE-FO Data

Six GRACE/GRACE-FO solutions were derived from the Center for Space Research at the University of Texas at Austin (CSR), the Helmholtz Centre Potsdam-German Research Centre for Geosciences (GFZ), the Jet Propulsion Laboratory (JPL) and the Institute of Geodesy at the Graz University of Technology (ITSG), which were used to obtain the

monthly $1^\circ \times 1^\circ$ TWSC gridded data. To improve the accuracy of TWSC results, we performed coefficient replacement, filtering processing and scale restoration on four spherical harmonic (SH) solutions [28]. Moreover, we can also extract TWSC gridded data directly from two Mascon solutions from CSR and JPL. To maintain the continuity of TWSC, we used the dataset of reconstructed TWSC data in China based on PPT (2002–2019) to fill the 11-month data gap between GRACE and GRACE-FO missions [5,29]. For convenience, we availed two simplifications: (1) GRACE and GRACE-FO were collectively referred to as GRACE; (2) the four SH and two Mascon solutions were referred to as CSR-SH, GFZ-SH, JPL-SH, ITSG-SH, CSR-M and JPL-M, respectively.

3.1.2. ERA5 Dataset

ERA5 is the fifth-generation atmospheric reanalysis dataset of European Center for Medium-Range Weather Forecasts for the global climate from 1950 to the present, which is produced by ECMWF's Copernicus Climate Change Service. ERA5 provides monthly estimates of a large number of atmospheric, terrestrial and oceanic climate variables, covering Earth on a 30 km grid and resolving the atmosphere using 137 altitudes from the surface to 80 km altitude [30]. In our study, the monthly $0.1^\circ \times 0.1^\circ$ PPT, SM, TEM and runoff gridded data during 2003 and 2022 are derived from ERA5 dataset. ERA5 has good applicability and relevance when compared with measured data in China [31].

3.1.3. Global Land Data Assimilation System Model

The Global Land Data Assimilation System 2.1 model is a global high-resolution land surface simulation system, which is jointly developed by the Goddard Space Flight Center and National Centers for Environmental Prediction. It can provide the global land surface data from 1979 to the present [32]. In our study, the monthly $1^\circ \times 1^\circ$ ET gridded data from 2003 to 2022 were provided by the GLDAS model. The model has great applicability across global basins, both in terms of seasonal variations and long-term trends [33].

3.1.4. Sea Surface TEM (SST)

The Extended Reconstructed Sea Surface TEM dataset is a global monthly SST dataset derived from the International Comprehensive Ocean Atmosphere Dataset, which is provided by the National Center for Environmental Information, and its spatial resolution is $2^\circ \times 2^\circ$ [34]. In our study, the monthly SST gridded data were provided by ERSSTv5, and Version 5 is the newest version of Extended Reconstructed Sea Surface TEM.

3.1.5. Climate Index

ENSO is a quasi-periodic climate type that occurs across the Pacific Ocean near the equator, that is, the changes in the interaction between atmosphere and ocean in the tropical Pacific Ocean. Although it originates in the tropics, it can change the global atmospheric circulation, and then it affects TEM and PPT everywhere [35,36]. Niño3.4 index is used to measure SST anomalies. When it exceeds 0.5 for five consecutive months, an El Niño event is considered to have occurred, and a La Niña event is considered to have occurred when it is below -0.5 for five consecutive months [3]. The monthly Niño3.4 index was derived from the National Oceanic and Atmospheric Administration in our study.

The Western Pacific Subtropical High (WPSH) is a permanent high-pressure circulation system over the Pacific Ocean, which has an important impact on Chinese climate. Its location and intensity vary with the seasons. In our study, the WPSH area and intensity indices (WAI and WII) were provided by the National Climate Centre at the China National Meteorological Administration.

3.1.6. Drought Index

To verify the reliability and validity of the WSDI, we introduced two recognized drought indices, which are SPEI and SCPDSI, respectively. SPEI comprehensively considers the impact of PPT and potential ET on drought, while SCPDSI mainly integrates the

relevant data, such as PPT, TEM and SM, and it is the improved version of the Palmer drought severity index and has strong applicability on a global scale [37–39]. In our study, the spatial resolution of monthly SPEI gridded data is $0.25^\circ \times 0.25^\circ$, and SPEI has three different time scale results (SPEI-03, SPEI-06 and SPEI-12), which were provided jointly by Pyrenean Institute of Ecology and Aula Dei Experimental Station [40,41]. The monthly $0.5^\circ \times 0.5^\circ$ SCPDSI gridded data were provided by the Climate Research Unit at University of East Anglia.

3.1.7. Reservoir and Runoff Data

In our study, the water levels of reservoir and runoff data are from Water Resources Monitoring Bulletin for Important Control Sections in the YRB provided by Changjiang Water Resources Commission of the Ministry of Water Resources. This bulletin includes water resource facts of important water system nodes, important reservoirs and major water transfer projects in the Yangtze River Basin, as well as monitoring information of water resource monitoring sections at some provincial boundaries and important water events.

The datasets in our study are listed in Table 2.

Table 2. Summary of the datasets in our study.

Dataset	Short Name	Time Span	Spatial Resolution	Temporal Resolution	Data Source
GRACE/ GRACE-FO SH	CSR GFZ JPL ITSG	2003–2022	$1^\circ \times 1^\circ$	Monthly	http://icgem.gfz-potsdam.de/home , accessed on 10 November 2023
GRACE/ GRACE-FO Mascon	CSR JPL	2003–2022	$0.25^\circ \times 0.25^\circ$ $0.5^\circ \times 0.5^\circ$	Monthly	https://www2.csr.utexas.edu/grace/RL05_mascons.html , accessed on 10 November 2023 https://grace.jpl.nasa.gov/data/get-data/ , accessed on 10 November 2023
PPT TEM SM	ERA5	2003–2022	$0.1^\circ \times 0.1^\circ$	Monthly	https://cds.climate.copernicus.eu/cdsapp#!/search?type=dataset , accessed on 10 November 2023
ET	GLDAS	2003–2022	$0.25^\circ \times 0.25^\circ$	Monthly	https://disc.gsfc.nasa.gov/datasets?keywords=GLDAS_NOAH025_M_2.1&page=1 , accessed on 10 November 2023
SST	-	2003–2022	$2^\circ \times 2^\circ$	Monthly	https://psl.noaa.gov/data/gridded/data.noaa.ersst.v5.html , accessed on 10 November 2023
WAI WII Ridgt WRP	-	2003–2022	-	Monthly	http://cmdp.ncc-cma.net/cn/index.htm , accessed on 10 November 2023
Niño3.4 index	ENSO	2003–2022	-	Monthly	https://www.cpc.ncep.noaa.gov/data/indices/ , accessed on 10 November 2023
Drought Index	SPEI	2003–2022	$0.25^\circ \times 0.25^\circ$	Monthly	https://spei.csic.es/database.html , accessed on 10 November 2023
	SCPDSI	2003–2022	$0.5^\circ \times 0.5^\circ$	Monthly	https://crudata.uea.ac.uk/cru/data/drought/ , accessed on 10 November 2023
Water Level Runoff	-	2019–2022	-	Monthly	http://www.cjw.gov.cn/zwzc/zjgb/ , accessed on 10 November 2023

3.2. Method

3.2.1. Data Integration

Due to different mathematical models and processing parameters, GRACE TWSCs from different institutions are not consistent [42,43]. The inconsistency leads to reduced reliability of study results. Therefore, we must reduce the adverse impact of this inconsistency on the study results. In our study, we first estimated the uncertainty of six GRACE TWSCs by using the generalized three-cornered hat method. The method can estimate relative uncertainty of different datasets without any prior information, but it needs at least three datasets. Finally, the least squares approach was used to integrate these six GRACE TWSCs based on the uncertainty results. For detailed calculation process, please refer to Refs. [44,45].

3.2.2. WSDI

The WSDI is a hydrological drought index based on GRACE TWSC, whose expression is as follows [46]

$$WSD_{i,j} = TWSC_{i,j} - TWSC_j^{mean} \quad (1)$$

$$WSDI_{i,j} = \frac{WSD_{i,j} - WSD_j^{mean}}{\sigma_{WSD_j}} \quad (2)$$

where $WSDI_{i,j}$, $WSD_{i,j}$ and $TWSC_{i,j}$ are the WSDI, water storage deficit (WSD) and TWSC for the j th month in the year i ; WSD_j^{mean} and $TWSC_j^{mean}$ are the average WSD and TWSC for j th month; σ_{WSD_j} is the variance in the WSD for j th month.

According to the drought severity, the droughts were divided into four categories (D1, D2, D3 and D4). D0 represents the region with no drought [21]. The drought severity is judged based on the values of the WSDI. Table 3 shows the drought category by the WSDI and SPEI.

Table 3. Drought category by WSDI.

Category	Description	WSDI
D0	No drought	$WSDI > 0$
D1	Light drought	$-1.0 < WSDI \leq 0$
D2	Moderate drought	$-2.0 < WSDI \leq -1.0$
D3	Severe drought	$-3.0 < WSDI \leq -2.0$
D4	Extreme drought	$WSDI \leq -3.0$

3.2.3. Drought Characteristics

In our study, the drought is defined as WSDI less than 0 for three consecutive months. Drought characteristics include duration, start and end time, severity, peak and drought area ratio (DAR) [23]. Duration represents the number of months of drought, peak magnitude represents the maximum WSDI during the drought and drought area percentage indicates the ratio of the area with a WSDI value less than 0 to the total area of the study region. The expression of drought severity is as follows [37]:

$$S = \bar{W} \times M \quad (3)$$

where S represents the drought severity, \bar{W} represents the average WSDI value during the drought and M represents the drought duration up to the calculation month.

3.2.4. Standardized TEMP Index

In our study, we used standardized TEMP index (STI) to evaluate high-TEMP weather. The expression of STI is as follows:

$$STI_{i,j} = \frac{TEM_{i,j} - TEM_j^{mean}}{\sigma_{TEM_j}} \quad (4)$$

where $TEM_{i,j}$ and $STI_{i,j}$ represent TEM and STI for the j th month in the year i , respectively; TEM_j^{mean} and σ_{TEM_j} represent the average of and variance in TEM for j th month. If STI is greater than 0.5 in the current month, it is considered that there is high-TEMP weather in this month [47]. A CHD event is defined as when a drought occurs in the month and high-TEMP weather occurs at the same time ($WSDI \leq 0$ and $STI \geq 0.5$) [48]. Table 4 shows the hot category by STI [49].

Table 4. Hot category by STI.

Category	Description	STI
E0	No hot	$STI < 0.5$
E1	Light hot	$0.5 \leq STI < 0.8$
E2	Moderate hot	$0.8 \leq STI < 1.3$
E3	Severe hot	$1.3 \leq STI < 1.6$
E4	Extreme hot	$1.6 \leq STI$

3.2.5. Weight Migration

The weight migration can reflect spatiotemporal trends and spatial aggregation characteristics of drought events [50]. The center of gravity of the drought is the center of drought based on the WSDI value of each grid point within the region where drought occurs. The expression is as follows [51]:

$$B = \frac{\sum_{i=1}^n WSDI_i \cdot B_i}{\sum_{i=1}^n WSDI_i}, L = \frac{\sum_{i=1}^n WSDI_i \cdot L_i}{\sum_{i=1}^n WSDI_i} \quad (5)$$

where B and L are the latitude and longitude of the center of gravity of the drought event, separately; $WSDI_i$, B_i and L_i are the WSDI, latitude and longitude of grid point, separately.

4. Results

4.1. Uncertainty of TWSC and WSDI Construction

We calculated the uncertainties of six GRACE TWSCs (CSR-SH, 1.21 cm; GFZ-SH, 1.40 cm; JPL-SH, 1.41 cm; ITSG-SH, 1.53 cm; CSR-M, 7.19 cm and JPL-M, 3.98 cm). We found that the uncertainties of the six TWSCs have large differences. Therefore, if a certain GRACE TWSC is used alone, the reliability of our result will be reduced. To avoid this situation, we fused six GRACE TWSCs in this study. Figure 2 shows the temporal evolution of the six GRACE TWSCs and fused TWSC result. It indicates that seven time series of TWSC have the same change trend, peaks and troughs. The fused TWSC result has a strong correlation with the six GRACE TWSCs (correlation coefficients greater than 0.92), and the fused TWSC result has a much smaller uncertainty value (0.65 cm) than the other GRACE TWSCs. Thus, the fused TWSC demonstrates good performance with the six GRACE TWSCs in the YRB, and it has higher accuracy. Figure 3 shows the spatial distribution of the uncertainties of the fused TWSC results in the YRB. The uncertainties in most of the regions are below 0.9 cm. The southeastern portion of PLRB demonstrated the greatest uncertainty (1.2 cm), while the smallest uncertainties (0.3 cm) are concentrated in the upper reaches of the JSRB and YLRB. Therefore, we used the fused TWSC for the subsequent study and called it GRACE TWSC.

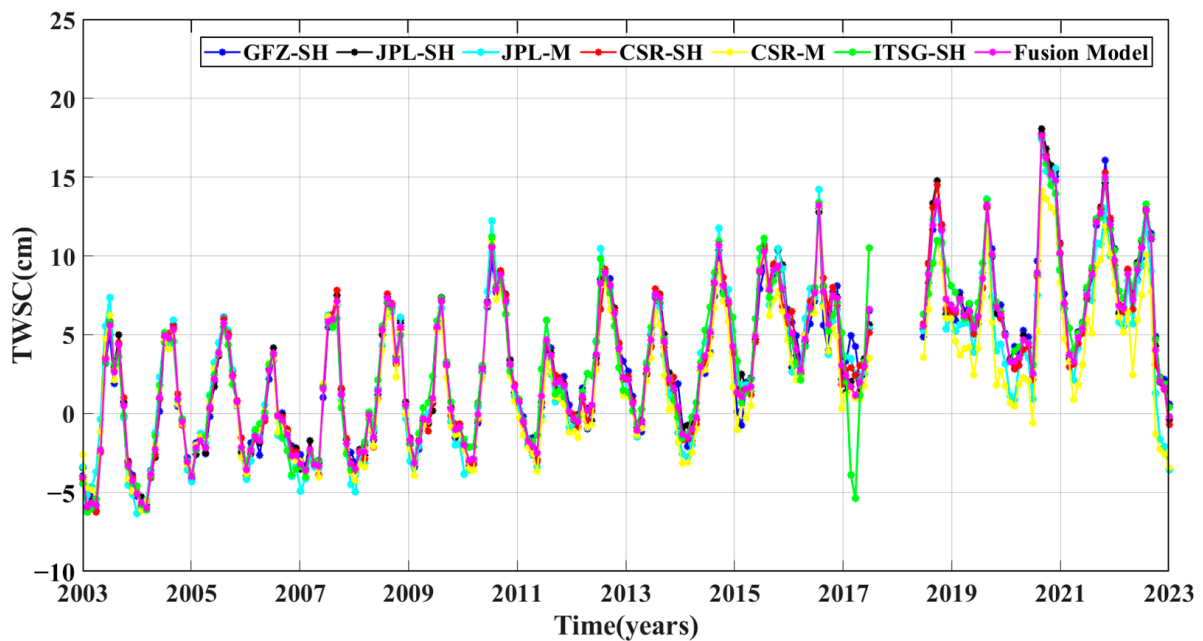


Figure 2. The time series of six GRACE TWSCs and fused results in the YRB during 2003 and 2022.

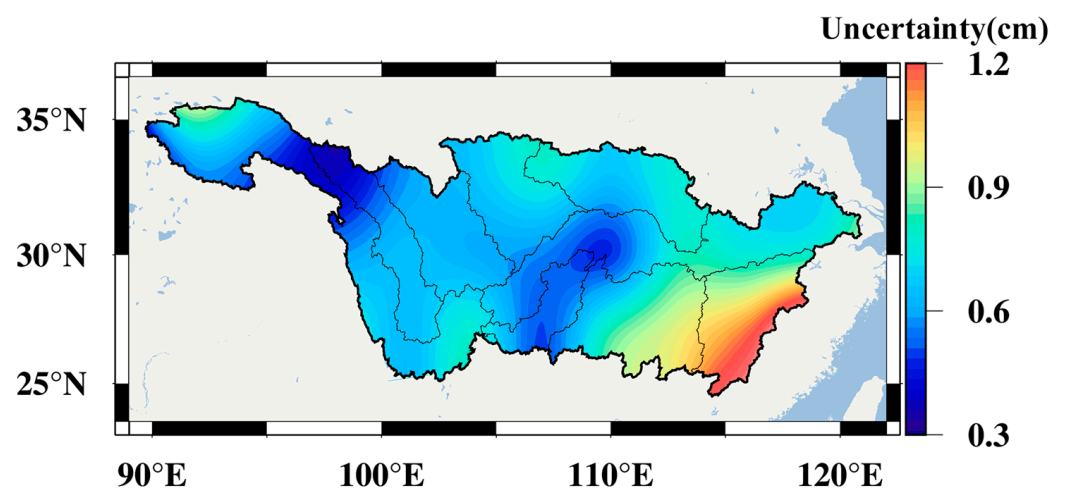


Figure 3. The spatial distribution of uncertainties of fused TWSC results in the YRB.

From Figure 2, we found that the fused TWSC results included a data gap (from July 2017 to May 2018), which caused great trouble for our study. Therefore, we used the reconstructed TWSC data to fill this gap to build a 20-year continuous uninterrupted TWSC. We used this continuous TWSC to estimate the WSDI values in the YRB during 2003 and 2020 and compared them to four traditional drought indices (SPEI-03, SPEI-06, SPEI-12 and SCPDSI). Figure 4 shows that the five drought indices have the same change trend and similar peaks and troughs. The correlation results indicate that the WSDI has a strong correlation with the four traditional drought indices (correlation coefficients greater than 0.5).

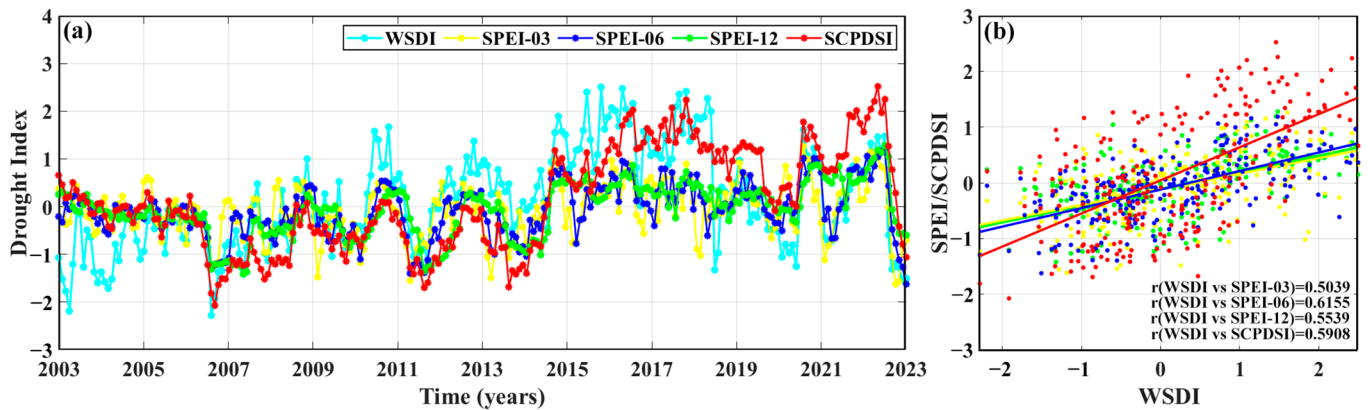


Figure 4. The time series of the WSDI, SPEI-03, SPEI-06, SPEI-12 and SCPDSI in the YRB during 2003 and 2022. In (b): the yellow points and line represent SPEI-03 vs. WSDI; the blue points and line represent SPEI-06 vs. WSDI; the green points and line represent SPEI-12 vs. WSDI; the red points and line represent SCPDSI vs. WSDI.

4.2. Spatiotemporal Evolution of the CHD Event

We calculated the TWSC and TEM anomalous values in the YRB during 2003 and 2022 (Figure 5a). The TEM anomaly was negative (-0.9 K) in May 2022, but it started to rise sharply since this month. The increasing trend continued until August and reached a peak (2.7 K). Although there were some recurrences from September to December, the TEM anomaly always remained above 0 K. As the TEM anomaly dropped to near 0 in December, it marked the end of the abnormal situation. During the study period, there were several WSD events in the YRB, and the worst WSD event occurred from July to December 2022. In this event, four months (from August to November) of the WSD exceeded -6 cm, and the maximum WSD (-7.2 cm) appeared in October. China's Flood and Drought Disaster Defense provided by the Ministry of Water Resources indicates that the YRB experienced the most severe meteorological and hydrological drought from July to October 2022 since 1961, when measured records became available, and locally it even lasted until December [52]. From Figure 5b, the STI and WSDI behaved exactly the same as the TEM and TWSC anomalies. During June and November 2022, the monthly STIs were greater than 0.5 , which means that the YRB experienced a high TEM event during this time period. Moreover, the study time can be divided into three periods: (1) the YRB was mainly dominated by droughts from 2003 to 2010; (2) floods were dominant from 2011 to 2018; and (3) droughts and floods occurred alternately during 2019 and 2022. During July and December 2022, a severe drought occurred in the YRB (WSDI values smaller than 0). Except for July, the WSDI values from July to December reached the moderate drought level. Among them, the WSDI in November reached its peak (-1.54).

Overall, this is a typical CHD event that began with hot weather followed by a drought, which lasted together for a period of time (five months), and the hot weather ended before the drought. CHD events lasting for such a long period of time are bound to cause great harm to local socio-economic development and the ecological environment. Therefore, the spatiotemporal evolution map of this event (Figures 6–8) helps us to better understand the formation and development of the CHD event.

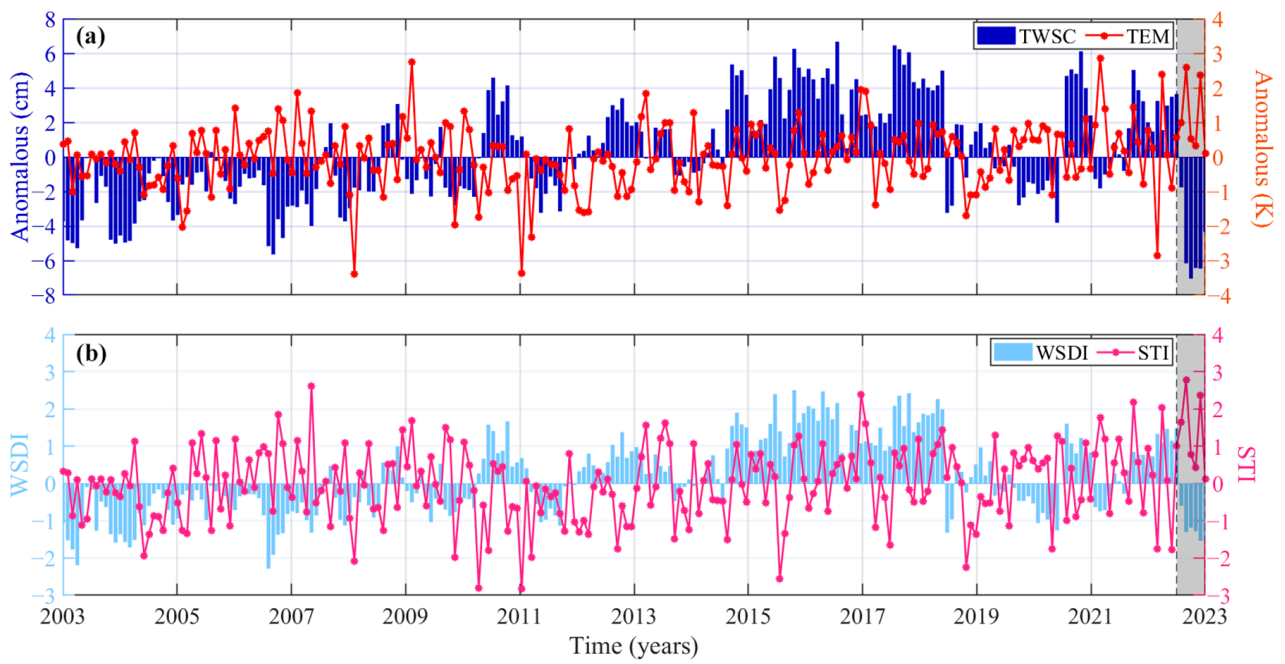


Figure 5. Temporal evolution of TEM and TWSC anomalies in the YRB during 2003–2022. (a) TWSC and TEM anomalous events; (b) the WSDI and STI; gray shading indicates compound hot and drought event occurrence.

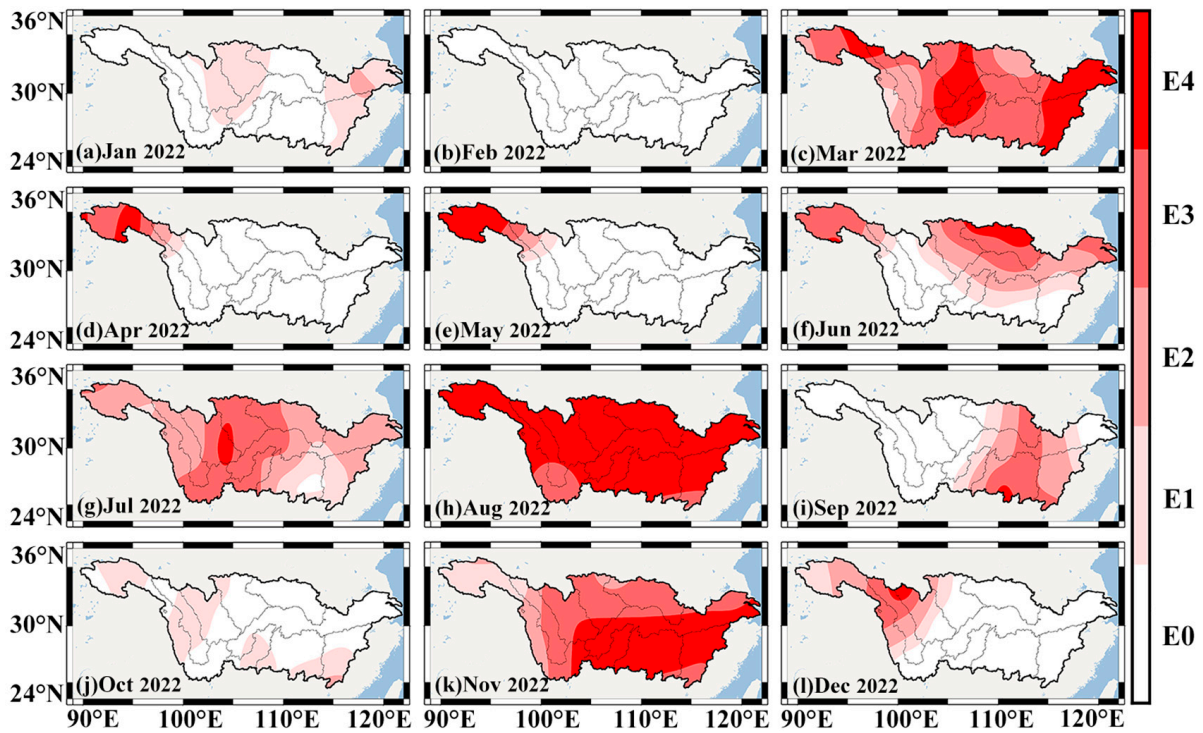


Figure 6. The spatiotemporal distribution of monthly STI in the YRB during January and November 2022.

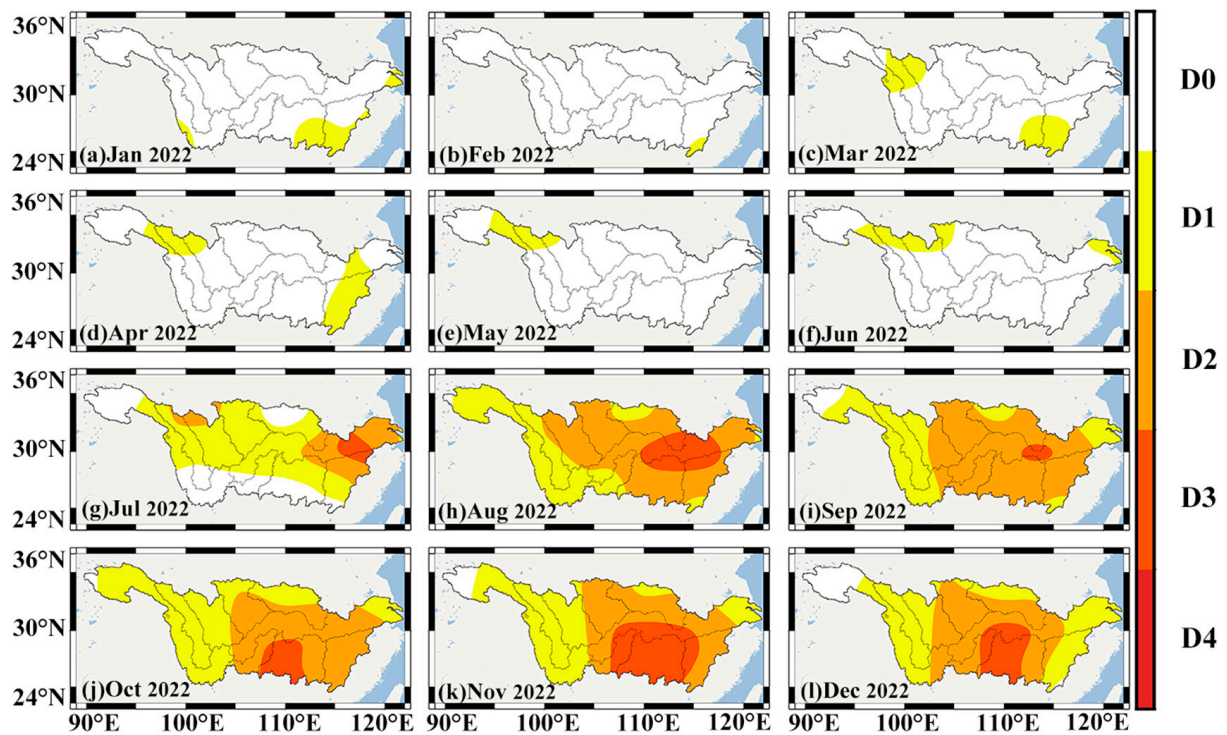


Figure 7. The spatiotemporal distribution of monthly WSDI in the YRB during January and November 2022.

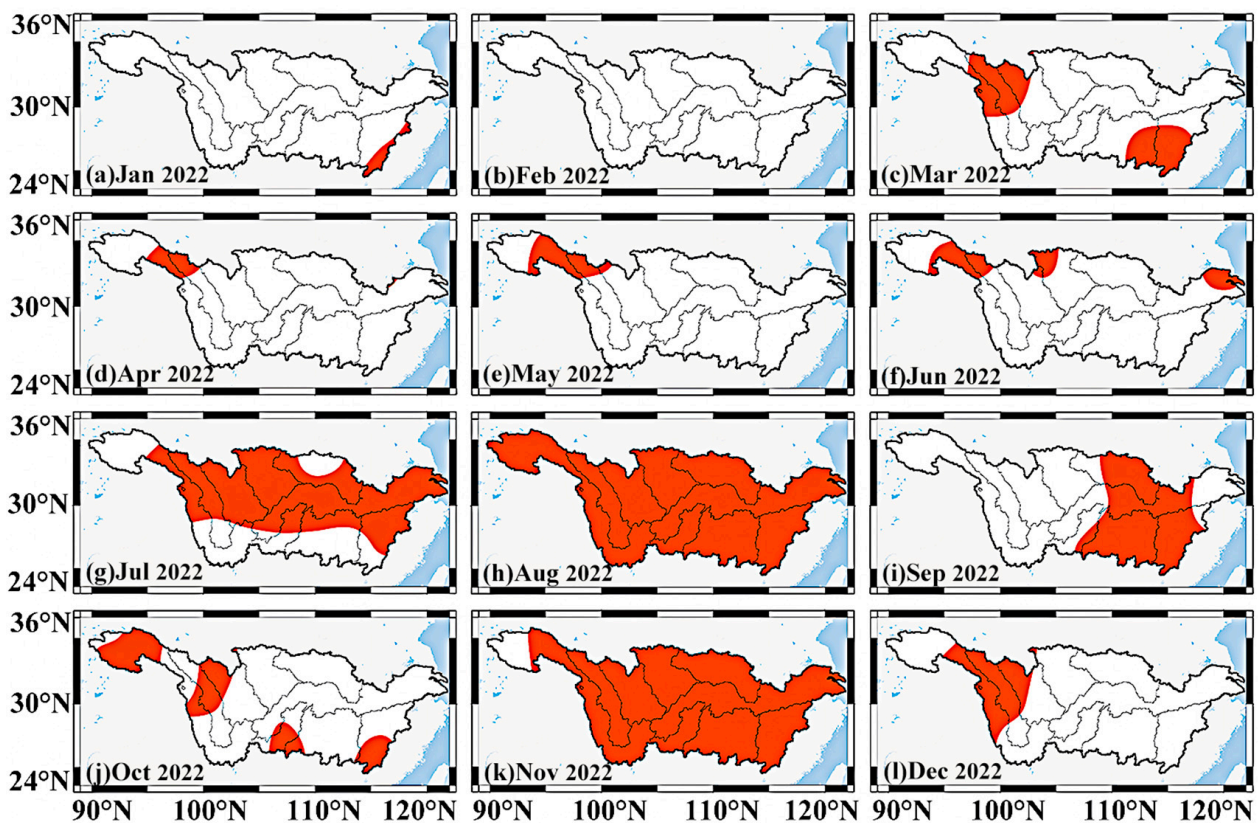


Figure 8. The spatiotemporal evolution of the CHD event in the YRB during January and November 2022. Dark red regions indicate the CHD event.

Figure 6 shows the spatiotemporal evolution of the hot weather in the YRB in 2022. In January, light hot occurred locally in the YRB, mainly in the MRB, JRB, PLRB and the lower reaches of the MSY. Small parts of the lower reaches of the MSY even experienced moderate hot. No hot appeared in the entire YRB in February. However, hot weather made a comeback in March, covering the entire YRB. Among them, the upper JSRB, the lower reaches of the MRB and JRB, PLRB and the lower reaches of the MSY experienced extreme hot. As we entered April, the hot weather subsided extensively, occupying only the upper reaches of the JSRB. In May, there was little change in the extent of hot weather, but the area affected by extreme hot was expanding. The range of hot weather expanded significantly in June, and by July it had basically covered the entire YRB, but this time it was mainly dominated by light and moderate hot. During August, the entire basin was dominated by hot weather and the vast majority of the regions were in extreme hot, with only a small portion of the southwest and southeast in severe hot. The effects of hot weather began to diminish in September; the trend continued into October. In November, hot weather again covered the YRB, but the severity was decreased compared to August. Extreme hot was mainly entrenched in the WRB, DLRB, PLRB, and MSY. The hot weather finally receded in December, but it still affected the northwest of the YRB. In summary, hot weather recurred throughout 2022 in the YRB, and, in July–August, the hot weather controlled the entire basin for two consecutive months, which suggests that the entire basin was in a hot-weather period for a full 60 days. This is an important reason for the occurrence of extreme drought.

From January to June, only small regions with light drought were observed in the YRB (Figure 7). From July to December, an extreme drought swept across the YRB. In July, most of the basins were under the grip of drought, and light drought dominated. Moderate drought occurred in the upper reaches of the YLRB and MRB and the lower reaches of the PLRB and MSY. Some parts of the lower reaches of the PLRB and MSY even experienced severe drought. After entering August, the drought covered almost the entire basin. The scope of influence of the moderate drought expanded significantly, occupying almost two thirds of the area, and severe drought also extended to the DLRB and HRB. By August, the YRB was still in the grip of drought, except for parts of the upper reaches of the JSRB. The range of moderate drought contracted, while that of extreme drought narrowed to parts of the MSY. In October, although the drought area widened, the area of moderate drought reduced significantly. Extreme drought shifted to the DLRB and expanded in size. By November, only parts of the upper reaches of the JSRB were out of the drought haze. The area of moderate and extreme drought expanded. While there was no significant change in the extent of drought in December, the extent of moderate and severe drought shrunk.

Figure 8 shows the spatiotemporal evolution of the CHD event in the YRB. From January and February, almost no CHD event is demonstrated in the YRB. During March and June, a CHD event occurred in the upper reaches of the JSRB and YLRB. Although other regions of the YRB also experienced brief periods of hot and dry climate during this time, they were too brief to constitute a CHD event. Beginning in July, a basin-wide CHD event appeared in the YRB. By August, the CHD event covered the entire basin. Although the impact of this event waned from September to October, it again evolved into a basin-wide event in November. As we entered December, the impact of this CHD event tapered off in the upper reaches of the JSRB, YLRB and MRB, meaning that the event had entered the closing phase.

We counted the performance of this CHD event in different sub-basins (Figure 9 and Table 5). Although the YRB experienced hot weather since June, not all the sub-basins were in it at the same time (Figures 5b and 9a). Among them, the JRB, WRB, HRB, DLRB and MSY started in June, while the other basins started in July. Almost all the basins experienced a sharp increase in STIs from June to August. The fastest rising STI was in the PLRB (1.26/month). After a peak in August, the hot weather showed significant fluctuations. By December, all but the JSRB, YLRB and MRB escaped the effects of the hot weather. In this process, the WRB experienced the longest hot weather period (6 months), but it was also the most severely affected (7.750). Moreover, the highest peak occurred in the JRB (2.496, E4). Overall, the lower and middle regions were more affected by the hot

weather. The drought behavior was generally consistent across all the basins (Figure 9b). Except for the YLRB, all the other basins entered drought in July. From June to July, the WSDI values displayed a sharp decline in all the basins, with a maximum drop of 2.103 (MSY). All the basins were in drought conditions and showed little variation in WSDI values during August and December. Among them, the DLRB was the most affected by the drought (−9.915) and has the highest peak (−2.492, D3). The WRB was the longest drought-affected area (6 months). In addition to the YLRB, the drought-affected areas of all the other basins reached 100.00% from August to December, and the hot-affected areas also reached 100.00% on several occasions. The above results indicate that the breadth of the CHD event impact on the YRB is unprecedented.

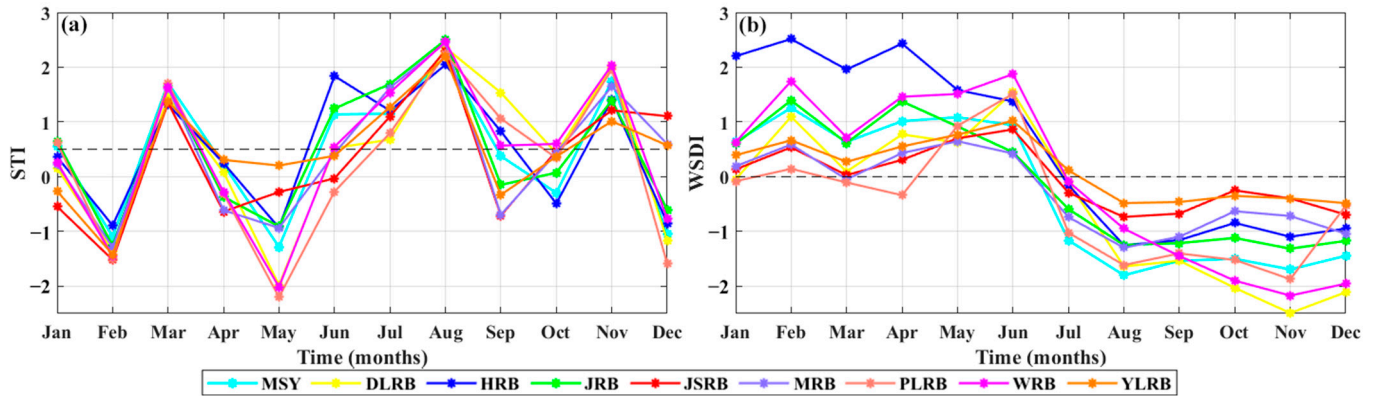


Figure 9. The temporal evolution of STI (a) and WSDI (b) in the nine sub-basins of the YRB during January and November 2022. The black dotted lines indicate STI = 0.5 (a) and WSDI = 0 (b).

Table 5. Characterization of 2022 CHD event in the YRB.

Region	Hot/Drought Duration (Months)	Peak		Severity		Max Area Ratio	
		Hot	Drought	Hot	Drought	Hot	Drought
YRB	4/6	2.276	−1.306 (November)	5.698	−6.356	100.00% (August)	99.39% (October)
JSRB	4/6	2.302	−0.736 (August)	4.613	−3.044	100.00% (August)	100.00% (August to December)
YLRB	4/5	2.185	−0.484 (December)	5.041	−2.177	100.00% (August)	96.90% (October)
MRB	4/6	2.445	−1.298 (August)	6.313	−5.527	100.00% (July, August, November)	100.00% (August to December)
JRB	4/6	2.496	−1.316 (November)	6.826	−6.663	100.00% (July, August, November)	100.00% (August to December)
WRB	6/6	2.467	−2.172 (November)	7.750	−8.520	100.00% (July, August, November)	100.00% (August to December)
HRB	5/6	2.044	−1.252 (August)	7.325	−5.458	100.00% (June, August, November)	100.00% (August to December)
DLRB	5/6	2.357	−2.492 (November)	7.105	−9.915	100.00% (August, September, November)	100.00% (August to December)
PLRB	4/6	2.242	−1.873 (November)	6.059	−7.967	100.00% (August, November)	100.00% (August to November)
MSY	4/6	2.201	−1.801 (August)	6.232	−9.143	100.00% (July, August, November)	100.00% (August to December)

To track the change trend of the CHD event, we mapped the center of gravity trajectories of drought and hot (Figure 10). We found that the center of gravity of the drought was essentially hovering at the intersection of the MSY, WRB and DLRB. As a result, these three basins are the most severe regions of the drought (Table 5, MSY, -9.143 ; WRB, -8.520 and DLRB, -9.915). The center of gravity of the hot area is relatively spread out. The center of gravity of the hot area in the first three months (June to August) is located in the JRB. It is a major cause of forest fires in Chongqing in August [53]. Subsequently, the center of gravity of hot moved successively to the DLRB (September), MRB (October) and the junction of the MSY and WRB (November). In general, the center of gravity of hot was still mainly concentrated at the junction of the middle and upper reaches of the YRB. Comparing Figure 10a,b, the trajectories of the drought and hot focus were roughly in the same regions during July and November. These are the regions that were hardest hit by the CHD event.

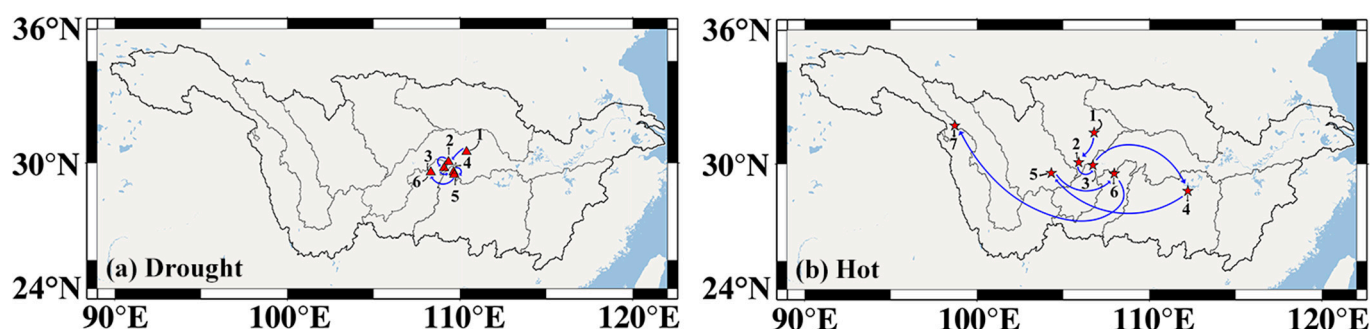


Figure 10. The center of gravity of hot and drought movement trajectory maps: (a) 1–6 represent the center of gravity of drought from July to December; (b) 1–7 represent the center of gravity of hot from June to December.

4.3. The Driving Factors of the CHD Event

In addition to high TEM, the main factor contributing to drought is PPT. From Figure 11, the percentages of PPT anomalies were negative several times during 2003 and 2022, and there are two main time periods with longer consecutive negative values (from January to May 2011 and from July to December 2022). Comparing the PPT performance at the two time periods, we can see that the duration and severity of negative PPT anomalies for the CHD event (red box, Figure 11) are the worst in the study period. From June to July, the PPT changed dramatically (anomaly percentage 3.05% to -32.04%). Then, the negative anomaly climbed all the way up. By September, the PPT anomaly percentage reached 60.18%. Although the PPT deficit eased in October and November, it remained above -40% in both cases. It finally peaked in December (-62.14%). The meteorological records show that, in July–August 2022, the PPT in the middle and lower reaches of the YRB and the Sichuan and Chongqing regions was 20–80% lower than that of the same period in normal years [7]. As the hot weather continued in June, the ET in the YRB was also higher than the same period of a normal year. The percentage of the ET anomaly was from 5.21% (June) to 14.77% (August). By September, the ET had a negative anomaly, which was caused by a continued decrease in PPT.

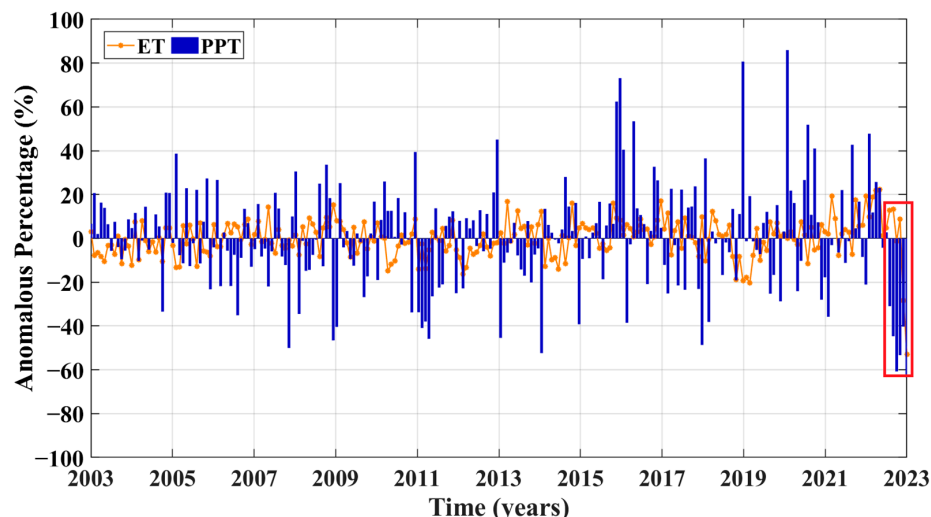


Figure 11. The percentages of PPT and ET anomalies in the YRB during 2003 and 2022. The red box indicates compound hot and drought event occurrence.

To analyze the performance of the PPT and ET in the different regions of the YRB during the CHD event, we plotted the spatial distribution map of the percentage of PPT and ET anomalies in the YRB (Figure 12). In June, parts of the YRB are in PPT deficit, mainly in the upper reaches of the JRB and the lower reaches of the HRB and MSY (Figure 12a). We found that the above regions largely overlapped with the regions with higher ET (Figure 12b). Moreover, Figure 6f shows that these regions are under hot weather. It explains that the high ET in the region is caused by high TEM. By July, the region with negative PPT anomalies extended to most of the YRB, and the percentage of PPT anomalies increased to over -80% in some regions (the middle reaches of the JSRB and YLRB, the middle and lower reaches of the MRB, JRB and HRB and the lower reaches of the PLRB, and MSY; Figure 12c), while the large regions were under the positive ET anomalies. Higher ETs are concentrated in the upper reaches of the YRB, especially in the lower reaches of the MRB, with the percentage of ET anomalies reaching more than 30% (Figure 12d). Due to the decreased PPT and higher ET, most of the YRB entered a state of drought (Figure 7g). In August, the PPT deficit in the middle and lower reaches of the YRB deteriorated further, with the vast majority of regions reaching a percentage of PPT anomaly of -80% or more (Figure 12e). The sub-basins of the upper reaches of the YRB are different. The PPT deficit eased in the upper and lower reaches of the JSRB, the lower reaches of the YLRB and the upper reaches of the JRB, while it intensified in the lower reaches of the MRB, JRB and WRB. During the same period, the ET showed a decreasing trend in the upper reaches of the YRB, but it showed an increasing trend in the middle and lower reaches (Figure 12f). Therefore, the drought severity was generally higher in the middle and lower reaches than in the upper reaches (Figure 7h). By September, the PPT deficit across the YRB was further exacerbated, especially in the DLRB, PLRB, the middle and lower reaches of the HRB, WRB and MSY, where the percentage of PPT anomaly reached -100% (Figure 12g). The high ET across the YRB showed a significant recession (Figure 12h) due to the easing of hot weather (Figure 6i) and continued decreased PPT. As a result, the drought severity eased in September, with a reduction in the regions of moderate and severe drought (Figure 7i). In summary, the high TEM and low PPT are the main drivers of the CHD event.

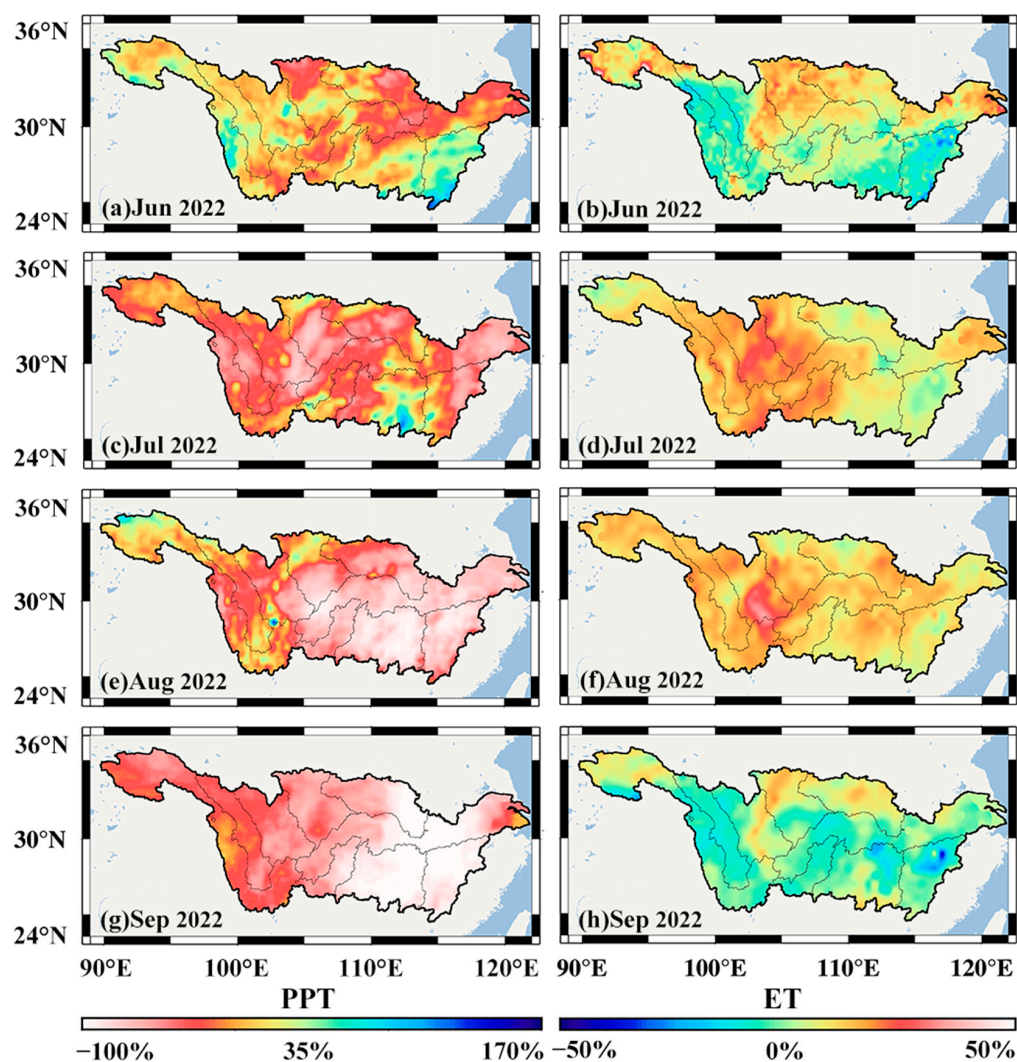


Figure 12. The spatial distribution map of anomalous percentages of PPT (a,c,e,g) and ET (b,d,f,h) in the YRB during July and December 2022.

5. Discussion

5.1. Extreme Climate Event

Why did the YRB experience such severe hot weather and low PPT in the summer of 2022? Anomalous changes in SST can indirectly affect atmospheric circulation through air–sea interactions. In the leadup to the CHD event, there were significant anomalous changes in SSTs in both the Indian and Pacific Oceans (Figure 13). In May 2022, the Indian Ocean SSTs showed a clear western low and eastern high, while anomalously low SSTs appeared in the east–central equatorial Pacific Ocean (Figure 13a). From June to August, the above two SST anomalies show a continuing trend of strengthening (Figure 13b–d). Moreover, these two SST anomalies are called negative Indian Ocean Dipole (IOD) and La Nina events by meteorologists. From May to August 2022, the IOD indices were -0.122 , -0.335 , -0.195 and -0.246 , respectively. Li et al. [54] indicated that the IOD can influence the Asian Summer Monsoon through the tropospheric flow field, South Asian High Pressure and WPSH. During the negative IOD event, a significant easterly anomaly was observed from the South China Sea to the Indian Ocean. The unusually active easterly winds in the south of China suppressed the water vapor transport in the South China Sea and the Bay of Bengal, resulting in unusually low PPT values in the YRB and nearby regions [55,56].

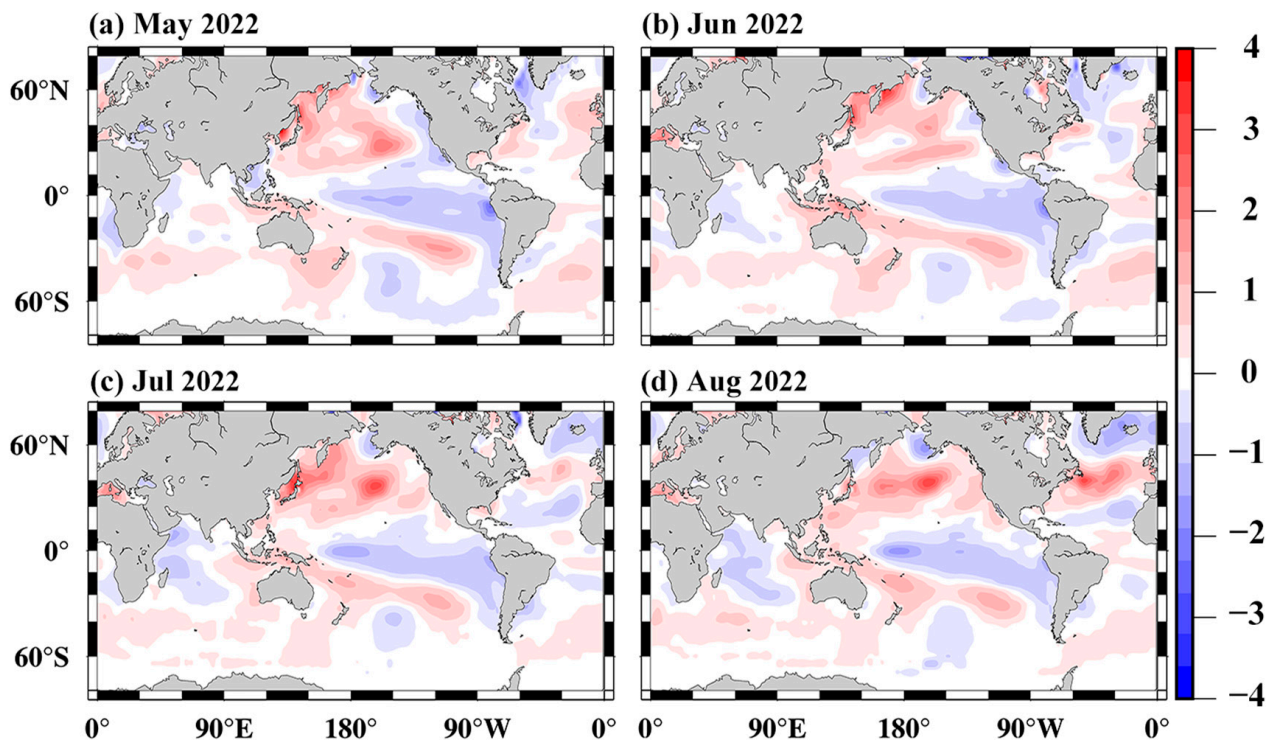


Figure 13. The spatial distribution map of global SST anomalous events (unit °C) during May and August 2022.

Previous studies show a negative correlation between the flood season PPT in the YRB and the SST in the equatorial western Pacific Ocean during the same period [23,57]. Low TEM in the tropical central Pacific can lead to suppressed convective activity in the region, inspiring a westward-transmitting Rossby wave train, which in turn enhances the WPSH. A La Niña event enhances the WPSH by increasing the frequency of anticyclones in the western Pacific, which in turn affects the PPT in the YRB [58]. Figure 14 shows a triple La Niña event that occurred during 2020 and 2022, which was last observed from 1998 to 2001. The occurrence of a triple La Niña event would greatly increase the probability of drought in the YRB. From July to November 2022, the WIIs were significantly higher than the average for the same period. Among them, the WII peaked in August (164.9), 64.9% above the average for the same period (Figure 15a). The WAI also far exceeded the average for the same period during July and August 2022, and it reached the maximum (456.3), which was 82.4% higher than the average for the same period (Figure 15b). It suggests that the WPSH in the summer of 2022 was exceptionally strong under the influence of the triple La Niña event. Figure 15c,d show that the ridge of the WPSH is more northerly than in previous years, while the WRP is more westerly. The position of the ridge reaches as far north as 30°N (August), and that of the WRP reaches 90°E at its westernmost point (August). It shows that the WPSH has a larger control range than in previous years and that both the northern and western boundary lines of the control range are much more northerly and westerly, respectively, than in previous years. Previous studies [8,59] indicate that, from July to August 2022, the WPSH and the Iranian High Pressure developed to a strong state and connected east–west, controlling the Tibetan Plateau to the YRB, resulting in an extensive warm high-pressure zone, leading to a drastic decrease in PPT and hot weather in the YRB. Overall, the WPSH is unusually stronger and larger during July and August 2022, and it controlled the YRB for a long period of time, resulting in the region being mainly affected by the subsiding airflow. Moreover, there is a very strong connection between the anomalous behavior of the WPSH and the triple La Niña event. Therefore, the triple La Niña event may be an important cause of the CHD event in the YRB.

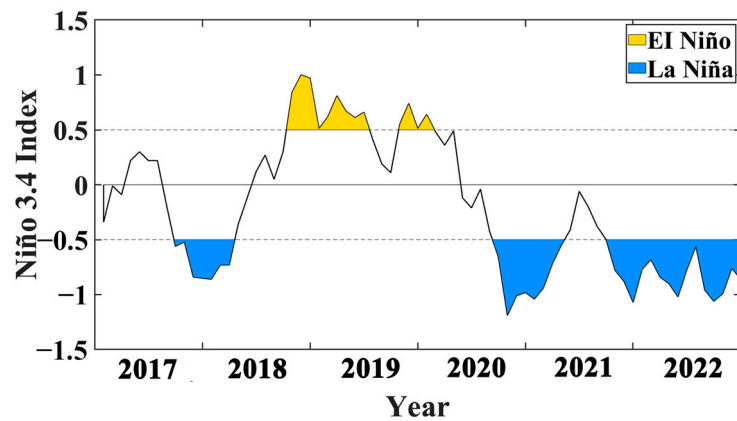


Figure 14. The temporal evolution of Niño 3.4 index during 2017 and 2022.

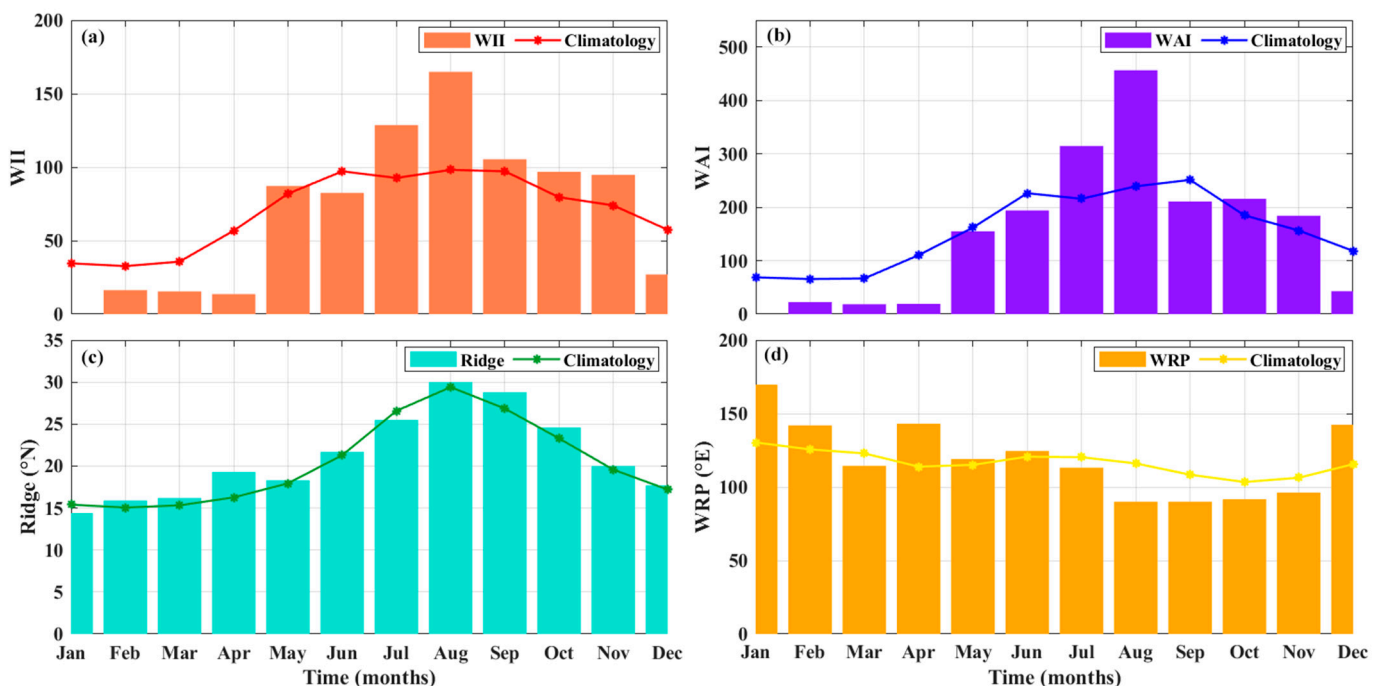


Figure 15. WII (a), WAI (b), Ridge (c) and WRP (d) in 2022. The lines represent the climatological state for the corresponding months from 2003 to 2022.

5.2. The Influence of the CHD Event

Meteorological drought is generally followed by agricultural drought, and the emergence of hydrological drought can have a direct impact on reservoir storage and water use, affecting the performance of irrigation projects. To assess the agricultural drought, we mapped the spatial distribution of the standardized SM index (SSI) in the YRB during July and December 2022 (Figure 16). In July, the agricultural drought ($SSI < -0.5$) is mainly concentrated in the upper reaches of the YRB, especially JSRB, YLRB and MRB (Figure 16a). By August, almost the entire YRB is under the grip of agricultural drought (Figure 16b). More than 4.42 million hectares of cropland are affected, and 4.99 million people and 920,000 heads of livestock had water difficulties [7]. To alleviate the impact of the drought on agricultural production, a group of reservoirs in the upper reaches of the YRB recharged 5.3 billion m^3 of water to the middle and lower reaches under the unified control [60]. From September to December, agricultural drought begins to recede, with the upper reaches of the YRB being the first to shake off the impact of the drought. However, the middle and lower reaches of the YRB have always been under the impact of agricultural drought (Figure 16c–f). The agricultural drought hits hardest mainly in the

WRB and the upper reaches of the MSY during October and December, which is consistent with hydrological drought (Figure 10a). To safeguard the demand for agricultural irrigation in the middle and lower reaches, a group of reservoirs in the YRB carried out the second drought replenishment operation in September, which totaled 2.59 billion m³ of water [60]. It may be one of the important reasons for the continued easing of agricultural drought in the middle and lower reaches of the YRB from October to December.

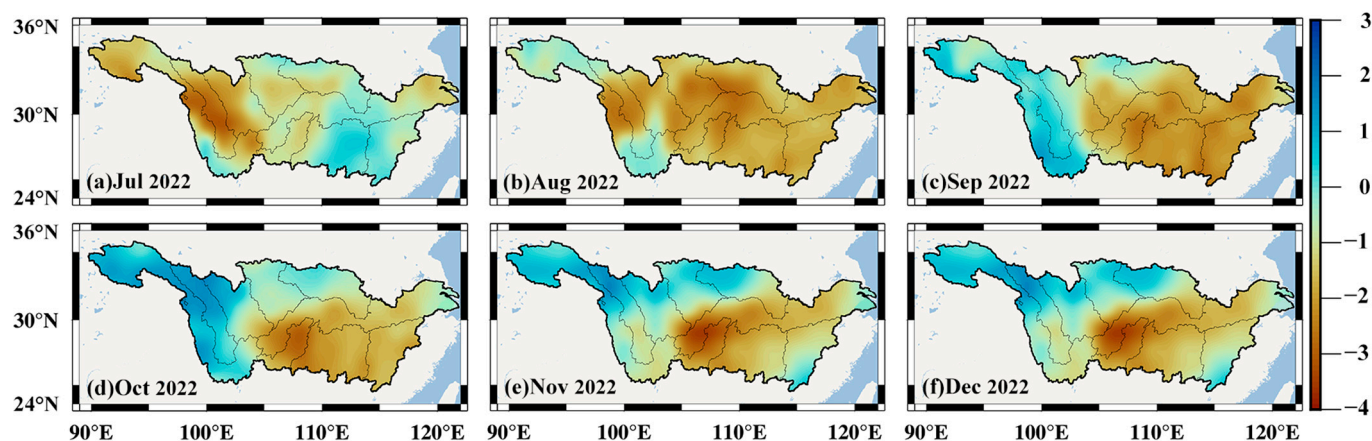


Figure 16. The spatial distribution map of SSI in the YRB during July and December 2022.

The CHD event not only adversely affected agricultural production but also seriously disrupted the daily production and livelihoods of the population. From Figure 17, we found that the monthly changes in water levels of the four reservoirs have the same pattern; that is, the highest water levels generally occur in October or November, while the lowest levels generally occur in April, May or June. This is because the reservoirs need to be emptied of stock before the flood season (May to October) and used to store more water during the flood season. Therefore, the water levels show an upward trend from June to October. However, the pattern was broken in 2022: the water levels of the Three Gorges, Jinping and Xiluodu reservoirs showed an initial decrease and then an increase, and that of Goupitan Reservoir showed a consistent downward trend. Moreover, the water levels of the four reservoirs were below average from July to December 2022. Compared to the same period of the last three years, the generation of Three Gorges and Xiluodu showed negative anomalies from early and late July, respectively, and the anomaly percentages of the two reservoirs reached 65% and 30% in late August, respectively [61]. The local news indicated that the severe drought resulted in a more than 50% reduction in the hydropower generating capacity of Sichuan, causing severe power shortages [62]. To ensure electricity for the daily lives of people, many large- and medium-sized enterprises have suspended power and production, and large shopping malls have taken measures to restrict electricity [63].

Drought has a serious impact on the water resources of the YRB. We found that the runoff from four hydrological stations showed a decrease rather than an increase in the flood season of 2022 (Figure 18). It is a significant departure from the performance of the same period in previous years. In July 2022, the increasing trend in runoff was abruptly broken and shifted from increasing to decreasing. Compared to the same period in previous years, the maximum values of the negative anomalies of the four hydrological stations appeared in September 2022, which are 59.32% (Xiangjiaba), 65.41% (Yichang), 69.63% (Hankou) and 71.61% (Datong), respectively. Guo et al. indicated that the natural water inflow of the upper reaches of the YRB was 35–52 billion m, about 20% less than the same period in the past five years [61]. The government's report demonstrated that the CHD event caused 810,000 people and 920,000 livestock to suffer from water shortages [52].

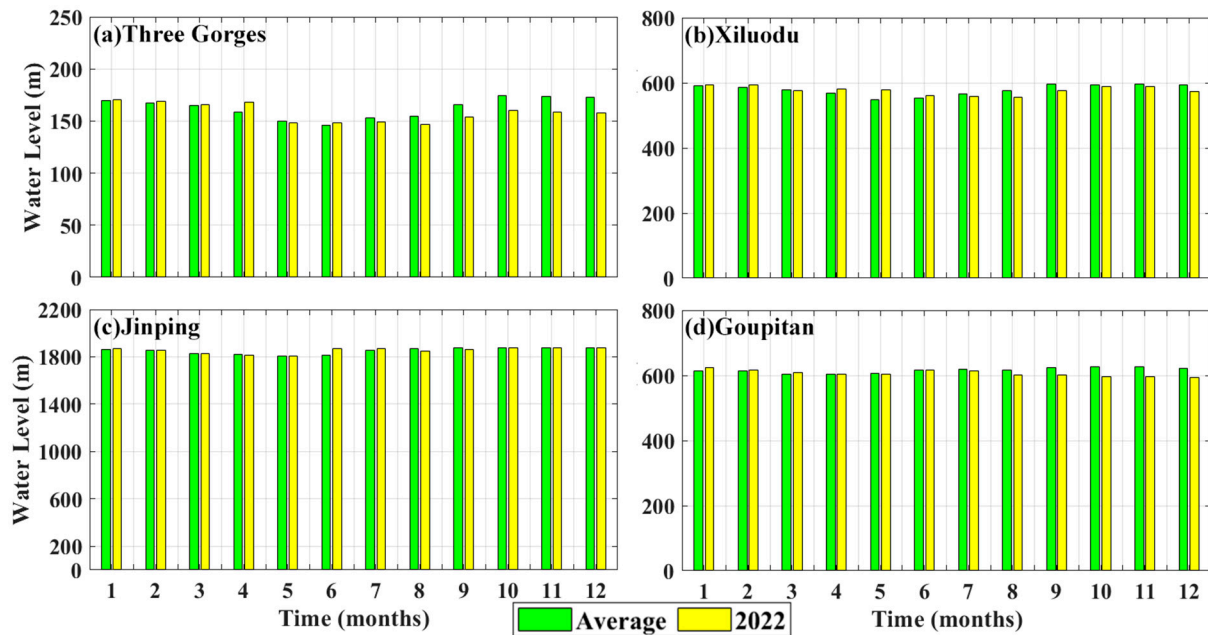


Figure 17. The monthly change in water level of four hydroelectric power stations in the YRB. The green and yellow bars indicate the averages for 2019–2021 and 2022, respectively.

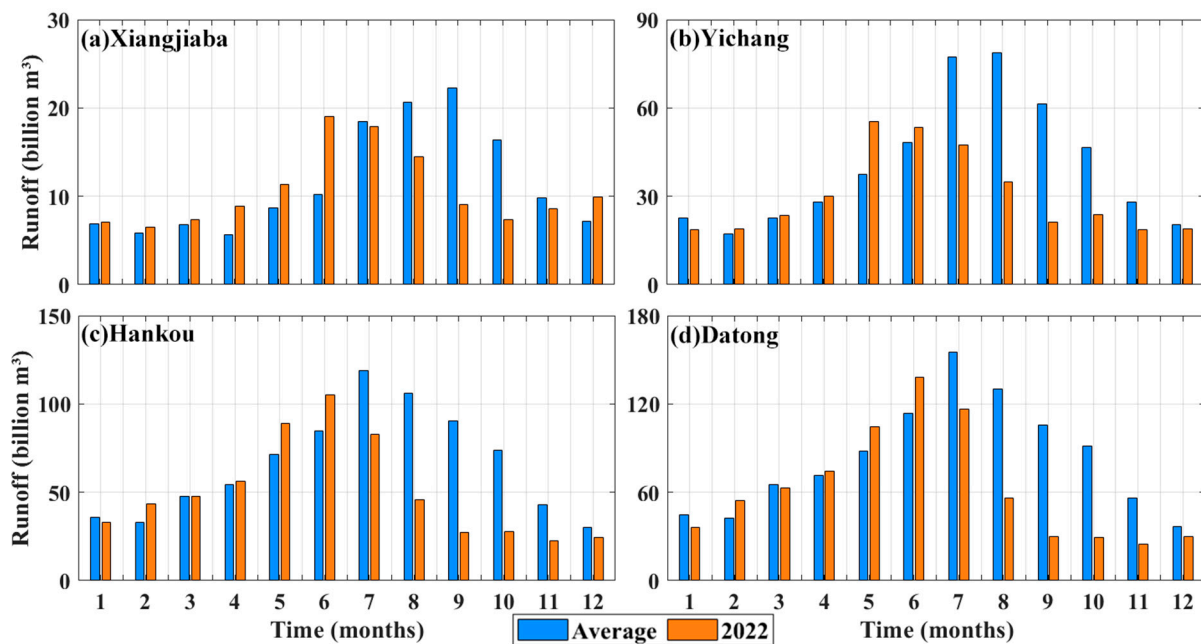


Figure 18. The monthly change in runoff of four hydrological stations in the YRB. The blue and orange bars indicate the averages for 2019–2021 and 2022, respectively.

6. Conclusions

In this study, we applied the GRACE/GRACE-FO, meteorological, hydrological and satellite remote sensing data to investigate the spatiotemporal characteristics of the CHD event in the YRB in 2022 in order to study the physical mechanism of its formation and discuss the damage caused by it. Our study results are summarized as follows:

Firstly, we fused six GRACE/GRACE-FO solutions to improve the accuracy of the TWSC, and the fused TWSC results were used to estimate the WSDI time series in the YRB during 2003 and 2022. The WSDI was validated and proved its applicability and reliability in the YRB.

Secondly, we used the WSDI and STI to characterize the spatiotemporal evolution of the CHD event. The results show that the drought severity of this CHD event was the most severe during 2003 and 2022. The WRB, DLRB and MSY are the three regions most affected by this event, and the center of gravity of the event hovers at the junction of the three regions.

Finally, the CHD event is very closely connected to the global extreme climate events (La Niña and negative IOD events). Due to the global climate events, an unusually strong WPSH appeared in the YRB during the summer of 2022, which kept the YRB and its neighboring regions in a permanent state of high TEM and blocked moist air from the sea. The perpetuation of this situation led to this CHD event. Moreover, the CHD event caused the emergence of widespread and prolonged agricultural drought, as well as a shortage in hydropower due to insufficient water storage in reservoirs, which seriously affected industrial production and the daily lives of individuals.

Our results can help to improve the understanding of the physical mechanism of the impact of extreme climate events on floods and droughts, provide the scientific data support for local governments to resist floods and droughts and provide a theoretical basis for the establishment of an early warning mechanism for floods and droughts.

Author Contributions: Conceptualization, L.C. and J.A.; methodology, L.C. and L.Z.; data curation, J.M. and Y.L.; writing—original draft preparation, L.C. and L.Z.; writing—review and editing, L.C. and J.A.; visualization, J.M.; supervision, C.Z. and Y.L.; project administration, C.Z.; funding acquisition, L.C. All authors have read and agreed to the published version of the manuscript.

Funding: This research was funded by the National Natural Science Foundation of China (Grant No. 42171141), 2023 China Student Innovation Training Programme Project (202311079005, 202311079007, 202311079008).

Data Availability Statement: No new data were created or analyzed in this study. Data sharing is not applicable to this article.

Acknowledgments: We are grateful to CSR, GFZ and JPL for providing GRACE solution; the COST-G for providing Swarm solution; the European Center for Medium-Range Weather Forecasts for providing PPT, SM, TEM and runoff data; the Global Land Evaporation Amsterdam Model for providing ET data; the Goddard Space Flight Center for providing GLDAS-2.1 data; and the National Oceanic and Atmospheric Administration for providing climate index data.

Conflicts of Interest: The authors declare no conflicts of interest.

Abbreviation

YRB	Yangtze River Basin
PPT	Precipitation
ET	Evapotranspiration
TWSC	Terrestrial water storage change
SM	Soil moisture
WSD	Water storage deficit
CHD	Compound hot and drought
JSRB	Jingsha River Basin
YLRB	Yalong River Basin
MRB	Min River Basin
JRB	Jialing River Basin
HRB	Han River Basin
WRB	Wu River Basin
DLRB	Dongting Lake Rivers Basin
PLRB	Poyang Lake Rivers Basin
MSY	Mainstream of the YRB
SST	Sea Surface Temperature
TEM	Temperature

WPSH	Western Pacific Subtropical High
WAI	WPSH area indices
WII	WPSH intensity indices
DAR	Drought area ratio

References

- Mishra, A.; Singh, V. A review of drought concepts. *J. Hydrol.* **2010**, *391*, 202–216. [[CrossRef](#)]
- Vicente-Serrano, S.; Peña-Angulo, D.; Murphy, C. The complex multi-sectoral impacts of drought: Evidence from a mountainous basin in the Central Spanish Pyrenees. *Sci. Total Environ.* **2021**, *769*, 144702. [[CrossRef](#)] [[PubMed](#)]
- Cui, L.; Zhang, C.; Yao, C.; Luo, Z.; Wang, X.; Li, Q. Analysis of the influencing factors of drought events based on GRACE data under different climatic conditions: A case study in Mainland China. *Water* **2021**, *13*, 2575. [[CrossRef](#)]
- Smith, A.; Matthews, J. Quantifying uncertainty and variable sensitivity within the US billion-dollar weather and climate disaster cost estimates. *Nat. Hazards* **2015**, *77*, 1829–1851. [[CrossRef](#)]
- Zhong, Y.; Feng, W.; Humphrey, V.; Zhong, M. Human-Induced and Climate-Driven Contributions to Water Storage Variations in the Haihe River Basin, China. *Remote Sens.* **2019**, *11*, 3050. [[CrossRef](#)]
- Buda, S.; Huang, J.; Fischer, T. Drought losses in China might double between the 1.5°C and 2.0°C warming. *Proc. Nat. Acad. Sci. USA* **2018**, *115*, 10600–10605.
- Xia, J.; Chen, J.; She, D. Impact and countermeasures of extreme drought in the Yangtze River basin in 2022. *Shuili Xuebao* **2022**, *53*, 1143–1153. (In Chinese)
- Zhou, J.; Ren, H.; Wang, M.; Cui, T. Analysis on the characteristics and causes of the drought in the Yangtze River basin in the summer of 2022. *Yangtze River* **2023**, *54*, 29–35. (In Chinese)
- Heim, R. A review of twentieth-century drought indices used in the United States. *Bull. Am. Meteorol. Soc.* **2002**, *83*, 1149–1166. [[CrossRef](#)]
- Aghakouchak, A.; Farahmand, A.; Melton, F.; Teixeira, J.; Anderson, M.; Wardlow, B.; Hain, C. Remote sensing of drought: Progress, challenges and opportunities. *Rev. Geophys.* **2015**, *53*, 452–480. [[CrossRef](#)]
- Rodell, M.; Famiglietti, J.; Wiese, D.; Reager, J.; Beaudoin, H.; Landerer, F.; Lo, M. Emerging trends in global freshwater availability. *Nature* **2018**, *557*, 651–659. [[CrossRef](#)] [[PubMed](#)]
- Zou, Z.; Li, Y.; Cui, L.; Yao, C.; Xu, C.; Yin, M.; Zhu, C. Spatiotemporal evaluation of the flood potential index and its driving factors across the Volga River basin based on combined satellite gravity observations. *Remote Sens.* **2023**, *15*, 4144. [[CrossRef](#)]
- Tapley, B.; Bettadpur, S.; Ries, J.; Thompson, P.; Watkins, M. GRACE measurements of mass variability in the Earth system. *Science* **2004**, *305*, 503–505. [[CrossRef](#)] [[PubMed](#)]
- Cui, L.; Zhu, C.; Wu, Y.; Yao, C.; Wang, X.; An, J.; Wei, P. Natural- and human-induced influences on terrestrial water storage change in Sichuan, Southwest China from 2003 to 2020. *Remote Sens.* **2022**, *14*, 1369. [[CrossRef](#)]
- Yirdaw, S.Z.; Snelgrove, K.R.; Agboma, C.O. GRACE satellite observation of terrestrial moisture changes for drought characterization in the Canadian Prairie. *J. Hydrol.* **2008**, *356*, 84–92. [[CrossRef](#)]
- Wang, J.H.; Jiang, D.; Huang, Y.H.; Wang, H. Drought analysis of the Haihe river basin based on GRACE terrestrial water storage. *Sci. World J.* **2014**, *2014*, 578372. [[CrossRef](#)] [[PubMed](#)]
- Yi, H.; Wen, L.H. Satellite gravity measurement monitoring terrestrial water storage and drought in the continental United States. *Sci. Rep.* **2016**, *6*, 19909. [[CrossRef](#)] [[PubMed](#)]
- Cui, L.; Zhang, C.; Luo, Z.; Wang, X.; Li, Q.; Liu, L. Using the local drought data and GRACE/GRACE-FO data to characterize the drought events in Mainland China from 2002 to 2020. *Appl. Sci.* **2021**, *11*, 9594. [[CrossRef](#)]
- Zhang, D.; Zhang, Q.; Werner, A.; Liu, X. GRACE-based hydrological drought evaluation of the Yangtze River basin, China. *J. Hydrometeorol.* **2016**, *17*, 811–828. [[CrossRef](#)]
- Wu, T.; Zheng, W.; Yin, W.; Zhang, H. Spatiotemporal characteristics of drought and driving factors based on the GRACE-derived total storage deficit index: A case study in Southwest China. *Remote Sens.* **2021**, *13*, 79. [[CrossRef](#)]
- Sun, Z.; Zhu, X.; Pan, Y.; Zhang, J.; Liu, X. Drought evaluation using the GRACE terrestrial water storage deficit over the Yangtze River basin, China. *Sci. Total Environ.* **2018**, *634*, 727–738. [[CrossRef](#)] [[PubMed](#)]
- Ran, Y.; Zhong, M.; Chen, W.; Zhong, Y.; Feng, W. Monitoring the extreme drought in the middle and lower reaches of the Yangtze River in 2019 from GRACE-FO satellites. *Chin. Sci. Bull.* **2021**, *66*, 107–117. (In Chinese) [[CrossRef](#)]
- Chao, N.; Wan, X.; Zhong, Y.; Yin, W.; Yue, L.; Li, F.; Hu, Y.; Wang, J.; Chen, G.; Wang, Z.; et al. Reconstructing a new terrestrial water storage deficit index to detect and quantify drought in the Yangtze River basin. *J. Hydrol.* **2023**, *625*, 129972. [[CrossRef](#)]
- Luo, H.; Huang, X. Research on the utilization and influence of water resource in grain production in main grain areas. *Agricul. Econ.* **2020**, *3*–5. (In Chinese)
- Cui, L.; He, M.; Zou, Z.; Yao, C.; Wang, S.; An, J.; Wang, X. The influence of climate change on droughts and floods in the Yangtze River basin from 2003 to 2020. *Sensors* **2022**, *22*, 8178. [[CrossRef](#)] [[PubMed](#)]
- Ji, X.; Tan, P.; Liu, Y.; Fu, J.; Wang, T. Research status of ecological operation of cascade hydropower stations in the upper Yangtze River basin. *Adv. Sci. Technol. Water Resour.* **2022**, *42*, 8–14. (In Chinese)
- Zhang, J.; Gao, Y.; Xu, W.; Xiong, K.; Du, L. Spatial and temporal analysis of extreme precipitation events in Yangtze River basin. *Yangtze River* **2019**, *50*, 81–86. (In Chinese)

28. Cui, L.; Yin, M.; Huang, Z.; Yao, C.; Wang, X.; Lin, X. The drought events over the Amazon River basin from 2003 to 2020 detected by GRACE/GRACE-FO and Swarm satellites. *Remote Sens.* **2022**, *14*, 2887. [[CrossRef](#)]
29. Zhong, Y.; Feng, W.; Zhong, M.; Ming, Z. *Dataset of Reconstructed Terrestrial Water Storage in China Based on Precipitation (2002–2019)*; National Tibetan Plateau Data Center: Beijing, China, 2020.
30. Hersbach, H.; Bell, B.; Berrisford, P.; Hirahara, S.; Horányi, A.; Muñoz-Sabater, J.; Nicolas, J.; Peubey, C.; Radu, R.; Schepers, D.; et al. The ERA5 global reanalysis. *Q. J. Royal Meteorol. Soc.* **2020**, *146*, 1999–2049. [[CrossRef](#)]
31. Meng, X.; Guo, J.; Han, Y. Preliminary assessment of ERA5 reanalysis data. *J. Mar. Meteorol.* **2018**, *38*, 91–99. (In Chinese)
32. Rodell, M.; Houser, P.; Jambor, U.; Gottschalck, J.; Mitchell, K.; Meng, C.; Arsenault, K.; Cosgrove, B.; Radakovich, J.; Bosilovich, M.; et al. The Global Land Data Assimilation System. *Bull. Am. Meteorol. Soc.* **2004**, *85*, 381–394. [[CrossRef](#)]
33. Liu, R.; She, D.; Li, M.; Wang, T. Using satellite observations to assess applicability of GLDAS and WGHM hydrological model. *Geomat. Inf. Sci. Wuhan Univ.* **2019**, *44*, 1596–1604. (In Chinese)
34. Huang, B.; Thorne, P.; Banzon, V. Extended reconstructed sea surface temperature, version 5 (ERSSTv5): Upgrades, validations and intercomparisons. *J. Clim.* **2017**, *30*, 8179–8205. [[CrossRef](#)]
35. Zhou, T.; Yu, R.; Li, H.; Wang, B. Ocean forcing to changes in global monsoon precipitation over the recent half-century. *J. Clim.* **2008**, *21*, 3833–3852. [[CrossRef](#)]
36. Cayan, D.; Redmond, K.; Riddle, L. ENSO and hydrologic extremes in the western United States. *J. Clim.* **2010**, *12*, 2881–2893. [[CrossRef](#)]
37. Cui, L.; Chen, X.; An, J.; Yao, C.; Su, Y.; Zhu, C.; Li, Y. Spatiotemporal variation characteristics of drought and their connection to climate variability and human activity in the Pearl River basin, South China. *Water* **2023**, *15*, 1720. [[CrossRef](#)]
38. van der Schrier, G.; Barichivich, J.; Briffa, K.; Jones, P. A scPDSI-based global data set of dry and wet spells for 1901–2009. *J. Geophys. Res. Atmos.* **2013**, *118*, 4025–4048. [[CrossRef](#)]
39. Tegos, A.; Stefanidis, S.; Cody, J.; Koutsoyiannis, D. On the Sensitivity of Standardized-Precipitation-Evapotranspiration and Aridity Indexes Using Alternative Potential Evapotranspiration Models. *Hydrology* **2023**, *10*, 64. [[CrossRef](#)]
40. Vicente-Serrano, S.; Santiago, B.; Juan, I. A Multi-scalar drought index sensitive to global warming: The Standardized Precipitation Evapotranspiration Index—SPEI. *J. Clim.* **2010**, *23*, 1696–1718. [[CrossRef](#)]
41. Beguería, S.; Vicente-Serrano, S.; Angulo, M. A multi-scalar global drought data set: The SPEIbase: A new gridded product for the analysis of drought variability and impacts. *Bull. Am. Meteorol. Soc.* **2010**, *91*, 1351–1354. [[CrossRef](#)]
42. Zhang, B.; Liu, L.; Yao, Y.; van Dam, T.; Khan, S. Improving the estimate of the secular variation of Greenland ice mass in the recent decades by incorporating a stochastic process. *Earth Planet Sci. Lett.* **2020**, *549*, 116518. [[CrossRef](#)]
43. Cui, L.; Yin, M.; Zou, Z.; Yao, C.; Xu, C.; Li, Y.; Mao, Y. Spatiotemporal change in evapotranspiration across the Indus River basin detected by combining GRACE/GRACE-FO and Swarm observations. *Remote Sens.* **2023**, *15*, 4469. [[CrossRef](#)]
44. Long, D.; Pan, Y.; Zhou, J.; Chen, Y.; Hou, X.; Hong, Y.; Scanlon, B.; Longuevergne, L. Global analysis of spatiotemporal variability in merged total water storage changes using multiple GRACE products and global hydrological models. *Remote Sens. Environ.* **2017**, *192*, 198–216. [[CrossRef](#)]
45. Cui, L.; Luo, C.; Yao, C.; Zou, Z.; Wu, G.; Li, Q.; Wang, X. The influence of climate change on forest fires in Yunnan province, Southwest China detected by GRACE satellites. *Remote Sens.* **2022**, *14*, 712. [[CrossRef](#)]
46. Sinha, D.; Syed, T.; Famiglietti, J.; Reager, J.; Thomas, R. Characterizing drought in Indian using GRACE observations of terrestrial water storage deficit. *J. Hydrometeorol.* **2017**, *18*, 381–396. [[CrossRef](#)]
47. Hao, Z.; Aghakouchak, A. Multivariate standardized drought Index: A parametric multi-index model. *Adv. Water Resour.* **2013**, *57*, 12–18. [[CrossRef](#)]
48. Jiang, Y.; Hou, A.; Hao, Z.; Zhang, X.; Fu, Y.; Hao, F. Evolution of hot droughts in the Yangtze River basin in 2022. *J. Hydroelectr. Eng.* **2023**, *42*, 1–8. (In Chinese)
49. Cunha, A.; Buermann, W.; Marengo, J. Changes in compound drought-hot events over Brazil’s Pantanal wetland: An assessment using remote sensing data and multiple drought indicators. *Clim. Dyn.* **2024**, *62*, 739–757. [[CrossRef](#)]
50. Li, J.; Chunyu, X.; Huang, F. Land Use Pattern Changes and the Driving Forces in the Shiyang River Basin from 2000 to 2018. *Sustainability* **2022**, *15*, 154. [[CrossRef](#)]
51. Li, P.; Hu, Z.; Liu, Y. Shift in the trend of browning in Southwestern Tibetan Plateau in the past two decades. *Agric. For. Meteorol.* **2020**, *287*, 107950. [[CrossRef](#)]
52. China Ministry of Water Resource (CMWR). *China Flood and Drought Disaster Bulletin*; China Water Conservancy and Hydropower Press: Beijing, China, 2022.
53. A Fire Has not Been Extinguished and a Fire Has Started, Why Are These Frequent Hill Fires in Chongqing? Available online: <https://www.12371.gov.cn/Item/609868.aspx> (accessed on 26 November 2023).
54. Li, C.; Mu, M. The dipole in the equatorial Indian Ocean and its impact on climate. *Chin. J. Atmos. Sci.* **2001**, *25*, 433–443. (In Chinese)
55. Liu, X.; Yuan, H.; Guan, Z. Effects on ENSO on the relationship between IOD and China summer rainfall. *J. Trop. Meteorol.* **2008**, *24*, 502–506. (In Chinese)
56. Zhang, J.; Ye, C.; Chen, J.; Shen, W. Influence of the Indian Ocean Dipole on water vapor transport from southwesterly monsoon over the South China Sea in the summer. *Chin. J. Atmos. Sci.* **2019**, *43*, 49–63. (In Chinese)
57. Li, Z. EOF analysis of Pacific Ocean SST and China continental precipitation. *J. Guizhou Meteorol.* **2012**, *36*, 18–20. (In Chinese)

58. Li, Y.; Zhang, J.; Yue, P.; Wang, S.; Cha, P.; Wang, L.; Sha, S.; Zhang, L.; Zeng, D.; Ren, S.; et al. Study on characteristics of severe drought event over Yangtze River basin in summer of 2022 and its causes. *J. Arid Meteorol.* **2022**, *40*, 733–747. (In Chinese)
59. Xu, G.; Wu, Y.; Liu, S.; Cheng, S.; Zhang, Y.; Pan, Y.; Wang, L.; Dokuchits, E.; Nkwazema, O. How 2022 extreme drought influences the spatiotemporal variations of terrestrial water storage in the Yangtze River Catchment: Insights from GRACE-based drought severity index and in-situ measurements. *J. Hydrol.* **2023**, *626*, 130245. [[CrossRef](#)]
60. Zheng, J.; Zhang, H. Practice and consideration on drought relief joint operation of multi-reservoirs in Yangtze River basin in 2022. *Yangtze River* **2023**, *54*, 7–11. (In Chinese)
61. Guo, G.; Wu, Y.; Qin, P.; Liu, M.; Xia, Z.; Zhang, L.; Xue, H.; Feng, Y. Characteristics and cause analysis of extreme heat and drought event in Yangtze River basin during summer 2022 and impacts on hydropower resources. *Resour. Environ. Yangtze River* **2023**, *32*, 2098–2108. (In Chinese)
62. Drought in the Yangtze River Basin in 2022, with Rivers Breaking down in Many Provinces. Available online: <https://baijiahao.baidu.com/s?id=1746679602253257493&wfr=spider&for=pc> (accessed on 26 November 2023).
63. Why Is There a Power Shortage in Sichuan, a Major Hydropower Province? Available online: <https://www.sc.gov.cn/10462/10464/13722/2022/8/18/a041da76a6cd45b79b9f39d89b06187d.shtml> (accessed on 26 November 2023).

Disclaimer/Publisher’s Note: The statements, opinions and data contained in all publications are solely those of the individual author(s) and contributor(s) and not of MDPI and/or the editor(s). MDPI and/or the editor(s) disclaim responsibility for any injury to people or property resulting from any ideas, methods, instructions or products referred to in the content.